Electronic Materials Letters, Vol. 2, No. 2 (2006), pp. 73-86

Epitaxial Growth of Nano Quantum Dots by Metal-Organic Chemical Vapor Deposition

Weon Guk Jeong*

Department of Materials Engineering, Sungkyunkwan University, Suwon 440-746, Korea

The characteristics of the MOCVD epitaxial process and the physical properties of quantum wells (QW) are briefly discussed. The growth behavior of quantum dots (QD) through a self-assembling growth mode and the physical properties of the grown QDs are discussed with InP-based QDs. The InGaAs/InGaAsP QDs were grown at an areal density of the QDs as high as $1.1x10^{11}$ cm^{-2}. The FWHMs of the 10 K and room-temperature QD PL peaks were measured as 32 and 63 meV, respectively. The integrated PL intensity at room temperature was measured as 21% of that at 10 K. The threshold current density of the QD laser diodes (LD) was measured as 400 A/cm^{-2} per QD stack. A room temperature cw operation was achieved from ridgewaveguide (RW) QD LDs with five and seven QD stacks. All of the results show that the MOCVD growth condition has been optimized to yield top quality InP QDs thus far. however, the optical quality of these QDs is not as good as that obtainable from QWs mainly due to the nonuniformity in the sizes and compositions of the grown QDs. Nonetheless, the inhomogeneous broadening reported here due to the spread in QD size is beneficial to semiconductor optical amplifiers (SOA), and a high performance QD SOA has been demonstrated.

Keyword: MOCVD, Quantum Dots, InGaAs, InP, QD LDs, QD SOAs

1. INTRODUCTION

Many modern optoelectronic and electronic semiconductor devices utilize quantum effects in which the electrons and holes confined in nano-sized heterostrucutres show. The InP and GaAs based semiconductor laser diodes (LD) that are being used as light signal sources in optical fiber communication systems as well as the GaAs-based LDs that generate laser lights for DVD and CD players utilize quantum effects to generate optical signals at a bit rate of up to 10 Gbps, a high enough optical power to read and write digital codes on optical disks. GaAs-based High Electron Mobility Transistors (HEMT) that are being used as low-noise amplifiers for mobile phone handsets also utilize the quantum effects of the carriers formed at the interface between the high and low bandgap semiconductors. Recent developments of InGaN/GaN quantum wells (QW) on highly lattice mismatched sapphire substrates have realized the commercialization of high-brightness blue and green Light Emitting Diodes (LED). This has opened new markets for full-color displays and white LED lamps, which are expected to replace fluorescent and incandescent lamps for general lighting in the near future.

*Corresponding author: wgjeong@skku.ac.kr

The commercialization of the aforementioned high performance optoelectronic devices is possible through the development of epitaxial growth techniques such as Metal-Organic Chemical Vapor Deposition (MOCVD) and Molecular Beam Epitaxy (MBE). These growth techniques have been advanced to a stage that they provide fine control of the epitaxial layer thickness, down to a monolayer, that has led to precise control of the quantum well thickness. Furthermore, the growth of high quality three-dimensional nano-sized semiconductor islands has been demonstrated. This is opening up the possibility of fully extending the quantum effects to three dimensions. A further enhancement of the optoelectronic device performances is expected through the unique characteristics that the three dimensional quantum effects provide.

In this study, the characteristics of the MOCVD process and the physics of quantum wells are briefly reviewed. In addition, the status of the growth of quantum dots is discussed based on the experimental results.

2. MOCVD EPITAXIAL PROCESS

As the name suggests, the MOCVD process utilizes metal-organics (MO) as reactants for epitaxy. The term 'metal-organics' is used instead of then more common term 'organometallics', after the inventor who wanted to emphasize

that it is the metals not the organics that are to be used from the compound[1]. In MOCVD, the epitaxy of compound semiconductors occurs through a chemical reaction between metalorganics and hydrides, or between metalorganics. The former case is more common. It is desired that the epitaxial deposition process occurs only on wafer surfaces. Therefore, the source reactants are made to be inactive at room temperature and are delivered to a wafer surface that is heated to a higher temperature. In a subsequent step, the reactants undergo a thermal decomposition by heat, and the chemical reaction occurs on the wafer surface. Therefore, it is a cold-wall process in which only the wafer is heated while the rest of the growth chamber wall is kept cold.

The MOCVD process was proven to be a viable epitaxial process for growing device-quality compound semiconductor heterostructures as early as the late 1970's[2-6]. It was shown to be capable of producing such devices as high quality solar cells, detectors, and laser diodes that were comparable to the heterostructures grown by processes such as Liquid Phase Epitaxy (LPE), MBE and Chloride- and Hydride- Vapor Phase Epitaxy (VPE), the leading processes at that time. In addition, as the epitaxial structure of the optoelectronic devices became more complicated as the number of epilayers in one device structure became larger and the thickness of the epilayers became thinner in order to exploit the quantum effects, MOCVD and MBE became the processes of choice, as only these two processes were suitable for growing these complicated heterostructures.

In particular, the MOCVD technique is the most widely used technique for the mass production of quantum well structures. From among all techniques for producing quantum well structures, MOCVD provides many advantages. Among them are uniformity in the epilayer thickness and composition through the control of hydrodynamics, an abrupt heterostructure interface formation through a run-vent injection manifold, and various commercially available MO sources that lead to the growth of many different compound semiconductors that are incorporated into epitaxial device structures. Large-scale mass-production MOCVD reactors for the growing of LED structures on as many as forty two-inch wafers are currently commercially available.

A more detailed discussion concerning the MOCVD process can be found in review papers and monographs[7-9].

3. HETEROSTRUCTURES AND QUANTUM WELLS

When a semiconductor layer is sandwiched by layers with larger bandgap energy, as in Fig. 1(a), the electrons and holes fall into the layer with small bandgap energy. That is, the carriers are confined in the small bandgap semiconductor layer. Then, as the electrons and holes are located close to each other in the thin, small bandgap layer, the chances that the electrons and holes will collide and recombine increase. That is, the radiative recombination efficiency is enhanced by this double heterostructure (DH). In addition, the refractive index of a semiconductor small bandgap energy is larger than that with a larger bandgap energy. This waveguide structure effectively confines light into the small bandgap semiconductor and enhances the interaction that is needed for a stimulated emission of a laser between the carriers and light. These physical characteristics of the DH of the carrier and the optical confinement are the main forces that made the laser diodes to lase continuously at room temperature[10-12]. The same structure has been used to enhance the luminescence efficiency of LEDs.

When the thickness of a semiconductor with small bandgap energy is decreased until it is smaller than the de Broglie wavelength of the electron and hole in it, the motion of the carriers in the thickness direction is highly restricted. That is, the energy states that the carriers can have are not quasi-continuous as in bulk semiconductors, where the carrier motion is free. Instead, they can have only selected energy states; the energy states are quantized. In this case, the energy spacing

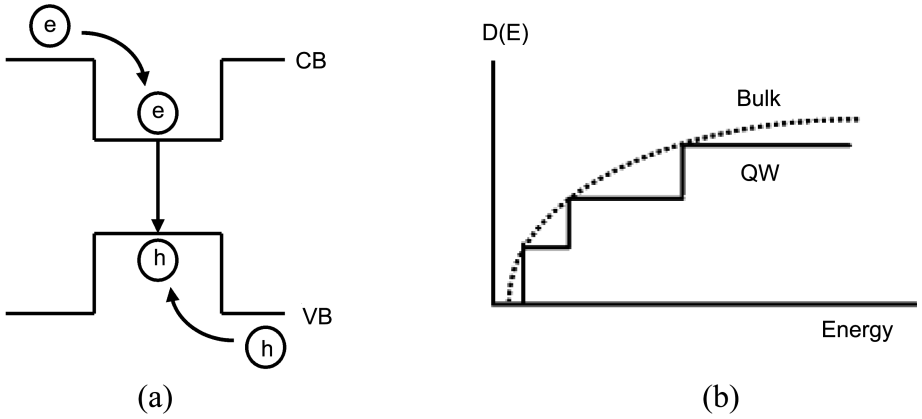

Fig. 1. (a) Carrier confinement and enhanced carrier recombination in a double heterostructure (DH). (b) Densities of energy states for bulk semiconductors and QWs.

between adjacent states becomes larger than the spacing between the states in bulk semiconductors. This effectively reduces the number of energy states that the carriers can occupy, as shown with the density of the states (DOS) in Fig. 1(b). Since the total number of carrier energy states is reduced, as carriers are supplied into the QW, the energy states are filled to higher states, with the same number of carriers as in bulk semiconductors. This causes the separation of the quasi-Fermi levels of the electrons and holes to be larger, so that the lasing threshold condition is satisfied with a smaller number of carriers compared to bulk semiconductors. In addition, the degeneracy of the heavy-hole (HH) and light-hole (LH) bands in bulk semiconductors is removed in QWs due to the difference in the effective masses of the heavy and light holes. The separation of the HH and LH bands further reduces the number of energy states in the valence band. This also helps to reduce the threshold current for lasing, as the carriers supplied to the QW fill up the higher energy states in the valence band more quickly[13]. Furthermore, when the QW layer is strained, the bandgap energy of the QW layer and the separation between the HH and LH bands changes. The hydrostatic component pushes the conduction band (CB) from the top of the valence band, and the shear component shifts the HH and LH bands. When the QW is compressively strained, the CB is pushed away from the valence band and the LH band is pushed to a higher energy state, while the HH band is pushed to a lower energy state in the valence band. When it is tensile strained, the CB band is pulled to the valence band and the HH band is shifted to a higher energy state, while the LH band is shifted to a lower energy state in the valence band[14]. Therefore, the number of energy states in the valence band can be further controlled by the strain in the QW layer. The de Broglie wavelength of electrons in III-V compound semiconductors is typically ~25 nm. Therefore, the QWs are grown to a thickness of approximately 10 nm in practice in order to fully utilize the quantization effects with well separated quantized energy states.

For HEMT structures, the quantized energy states increase the density of electrons at the interface between the high bandgap energy semiconductor and the low bandgap energy semiconductor. In addition, the carriers at the interface are away from the scattering centers of donor ions, thus the carrier mobility is larger than that in a bulk semiconductor. The higher carrier density and mobility as compared to those in bulk semiconductors lead to a larger current density that can transmit between the source and drain of the HEMTs, and a larger transconductance results[15].

All of the effects that can be obtained using the heterostructures and QWs are well understood, and most of the modern high performance compound semiconductor devices utilize QWs as their active layers in the structure.

4. QUANTUM DOTS

Efforts to further extend the quantum effects to two and three dimensions followed after the successful exploitation of the quantum effects in commercial compound semiconductor QW devices. Among several approaches, it was found that high quality quantum dots that exhibit three-dimensional quantum effects can be grown by utilizing the self-assembling behavior of highly strained semiconductor layers. When the semiconductor layer is grown on a substrate, the epilayer lattice works to maintain coherency with the substrate lattice. Specifically, the depositing atoms try to bond with the dangling bonds on the substrate in a one-to-one matching fashion. However, when the size of the epilayer lattice is different from that of the substrate lattice, the epilayer lattice is strained when maintaining coherency with the substrate. In this case, strain energy accumulates in the epilayer, and it increases with the thickness of the strained epilayer. When the strain energy in the epilayer becomes larger than the strain energy produced by a dislocation, coherency is broken and a dislocation is formed, as this state

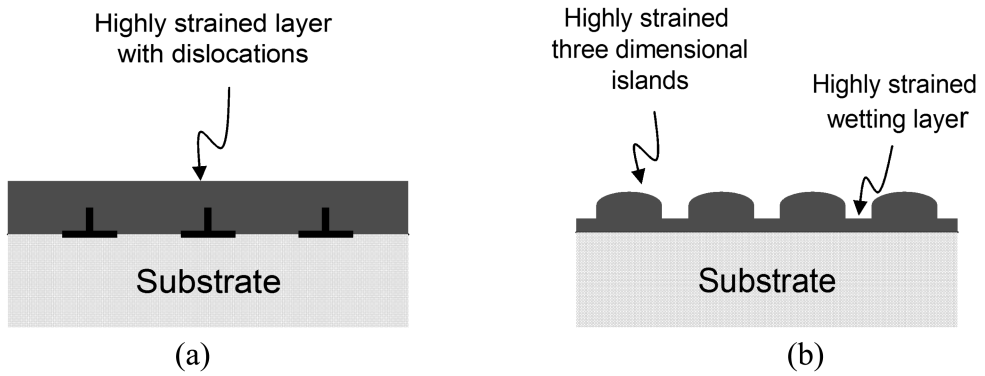

Fig. 2. (a) When the strain energy associated with a dislocation is smaller than the strain energy in the epilayer due to a difference in the lattice constant, a dislocation is formed to reduce the total strain energy in the epilayer. (b) Under appropriate growth conditions, three-dimensional islands are formed to reduce the total strain energy in the epilayer instead of the formation of dislocations.

with a dislocation is energetically more favorable than a strained state with coherency, as shown schematically in Fig. 2(a). However, when the growth condition is appropriately controlled, the highly strained layer breaks some of its bonds from the coherent state to reduce the strain energy. It forms, however, in three dimensional islands instead of forming dislocations as in Fig. 2(b). The formation of such three dimensional islands minimizes the strain energy in the epilayer in that it minimizes the bonding with the substrate lattice. This happens when the surface energy of the three dimensional island is smaller than the strain energy in a coherent state. In this way, high quality nano-sized three dimensional quantum dots (QD) are formed with a minimal number of crystal defects. This self-assembling growth mode is called the Stranski-Krastanow growth mode. It usually produces a thin wetting layer that maintains coherency with substrate lattice and the QDs on it. This growth mode has been extensively exploited for the growing of high quality QDs of GaAs, InP, and GaN based semiconductors. Especially for GaAs-based QDs, there is the additional advantage of using stained QDs. As the semiconductors that have large differences in the lattice constants can be grown as QDs, the choice of the band-gap energy of the QD semiconductor is expanded beyond those that cannot be grown as QWs. In fact, the research concerning GaAs-based QDs has been focused on extending the luminescence wavelength to 1.3 μm, the wavelength that is important for silica optical fiber communication systems[16-18]. With InGaAs QWs, the longest wavelength that can be achieved on a GaAs substrate with reasonable high quality is limited to ~1 μm. In contrast, an efficient method for forming two-dimensional quantum wires has yet to be found. Therefore, research concerning multi-dimensional quantum effects is focused mainly on quantum dots.

When the energy of carriers is quantized in three dimensions, there are no quasi-continuous energy states as in QWs and bulk semiconductors, and all of the energies have large energy spacings between them. The ideal density of energy state (DOS) for the quantum dots is shown in Fig. 3. As the energy states are largely spaced and discrete, when the carriers are supplied into the QDs they fill up the higher energy states with a smaller number of carriers as compared to QWs and bulk semiconductors. This leads to a reduced threshold current density for LDs. In addition, even when the carriers acquire thermal energy from the surroundings, if the thermal energy is not as large as the spacing between the energy states, the carrier cannot be transferred to a higher energy state. Therefore, the physical properties of QDs are much less sensitive in terms of temperature as compared to QWs and bulk semiconductors. A higher modulation speed of QD LDs is also expected from the high differential gain obtainable from the discrete DOS of QDs[19].

However, all of the ideal characteristics of QDs deteriorate in practice, as the QDs formed are not generally of the same

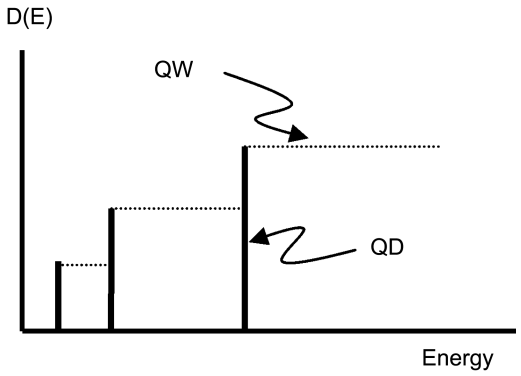

Fig. 3. Density of energy states for the QDs. The allowed quantized energies are discrete and thus form a delta-function-like shape.

size and composition but instead have non-uniformity. In the following chapter, the current status of the growth of QDs and the physical properties of the grown QDs will be discussed. The device results made from the grown QDs will also be discussed.

5. EXPERIMENTAL RESULTS ON THE GROWTH OF QDS

The InP-based QDs were grown on nominally exact (001) InP substrates by MOCVD operating at 76 torr. Trimethylindium (TMIn), trimethylgallium (TMGa), AsH_3 and PH_3 were used as source reactants, and SiH_4 and DMZn were used as doping reactants. When the substrate was loaded into the growth chamber, an InP buffer layer was grown at 620 °C. The temperature was then lowered and the QD as well as the barrier layer were grown. Typically, the QDs were grown at approximately 540 °C. The InAs and InGaAs were used as QD semiconductors, and InP and InGaAsP were used as barrier semiconductors. The properties of the QDs grown with different combinations of QD semiconductors and barrier semiconductors were compared. Multistacks of QDs were grown in order to study the effect of the spacer thickness between the QD layers. The spacer layer also functioned as a barrier layer for the QDs in this study. The luminescence wavelength and optical properties were optimized by controlling the compositions in the InGaAs QDs and the InGaAsP barrier layer, through variations in the spacing between QD stacks, as well as by changing growth conditions such as the growth temperature, the amount of TMIn and TMGa supply, the growth time, and the V/III ratio during the QD growth. The QD structure is schematically shown in Fig. 4(a).[20-27]

Atomic Force Microscope (AFM) images of the InAs QDs (QD3137) grown with an InP barrier on an InP substrate at 540 °C are shown in Fig. 5(a). It is shown that QDs were grown in a round, domed shape with an average diameter and height of 45 nm and 4.5 nm, respectively. The room

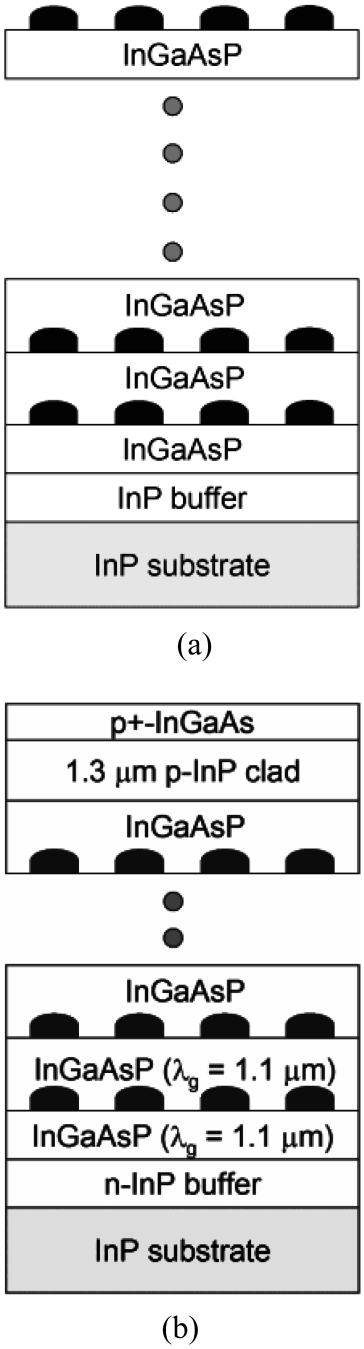

Fig. 4. (a) Structure of the QD multistacks for the AFM and PL measurements. (b) Structure of the QD LDs and SOAs with QD multistacks in the active layer.

temperature PL spectra of the InAs/InP QDs in Fig. 5(b) show that the luminescence wavelength can be controlled at approximately 1.55 μm by controlling the QD growth time. It is shown that as the QD growth time increases, the PL wavelength moves to a longer wavelength. This suggests that as the growth time increases, the size of the QDs increases, thus the quantization energy becomes smaller.

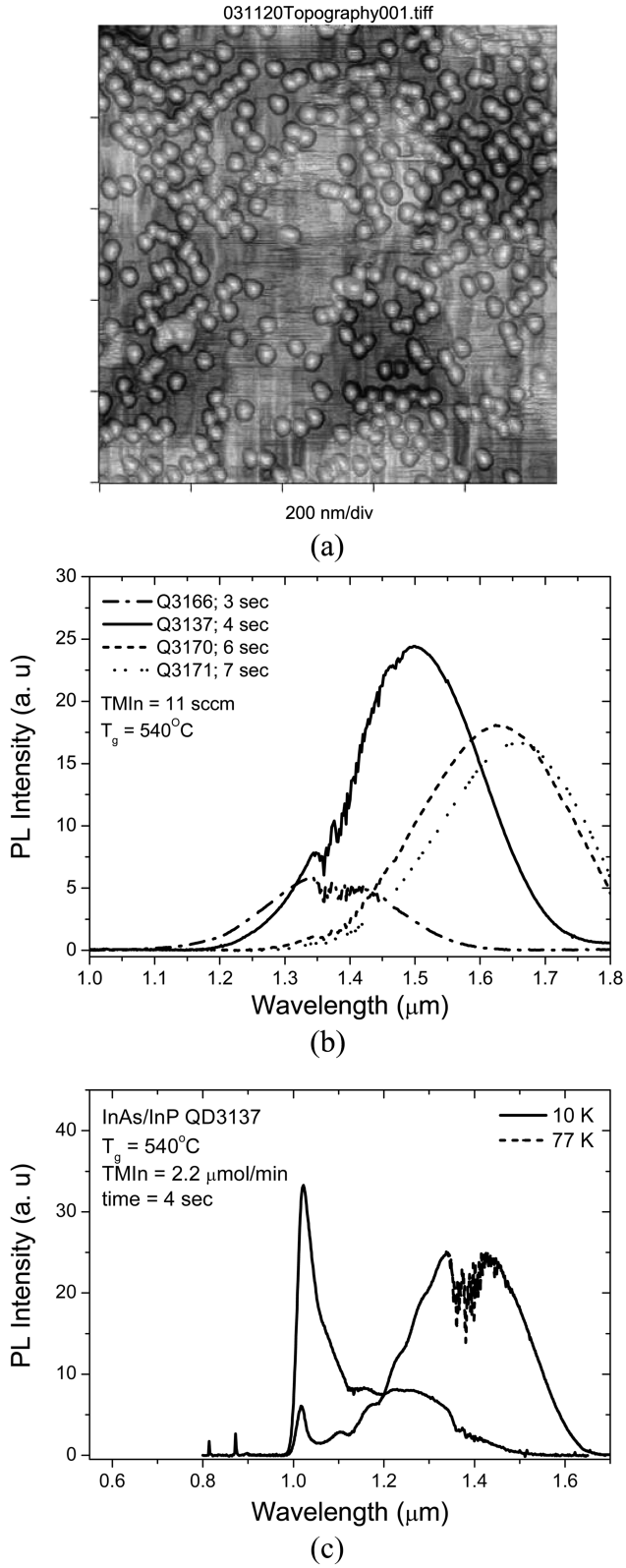

Fig. 5. (a) AFM image of InAs/InP QD3137 on (001) InP. The areal density is 2×10^{10} cm^{-2}. (b) Room temperature PL spectra of the InAs/InP QDs with differing growth times. (c) 10 K and 77 K PL spectra of InAs/InP QDs.

However, the low temperature PL spectra in Fig. 5(c) show that the optical properties of the grown InAs/InP QDs are not of high quality. The PL spectra measured at 10 K and 77 K show that the luminescence from the QDs is broad and that the luminescence from the wetting layer at ~1.02 μm is strong. This indicates that the size of the grown QDs is not uniform and that the photogenerated carriers do not effectively recombine in the QDs due to non-radiative recombination centers such as crystal defects in and/or around the QDs. However, it is worth noting that the shape of the QDs in Fig. 5(a) is round and dome-shaped, contrasting with previous reports in which the QDs were grown in an elongated form as quantum dashes rather than dots[28,29]. The QDs were grown in a more favorable shape for utilizing the three-dimensional quantum effects in this work.

In an effort to improve the optical quality of the QDs, InGaAs was used as a QD material. InGaAsP was used as a barrier for the InGaAs QDs, and the bandgap energy of the InGaAsP was controlled in accordance with the changes in InGaAs QD composition in order to maintain a luminescence wavelength to approximately 1.55 μm. The PL spectra of the QDs with the InGaAsP (λ_g = 1.0 μm) barriers are shown in Fig. 6. The QDs were grown at 540 °C for 3 sec, and the amount of TMIn supplied was 2.2 μmol/min. Five stacks of QDs were grown and were separated by 40 nm-thick InGaAsP. With the InAs QDs (QD3966), the PL wavelength was longer than 1.65 μm. In order to achieve a shorter QD PL wavelength with an identical InGaAsP barrier, Ga was incorporated into the QDs during the QD growth that would increase the bandgap energy of the QD material. The amounts of TMGa supplied were, 0.072 (QD3977), 0.18 (QD3979), and 0.24 (QD3972) μmol/min that results in Ga mole fractions of 2.6, 6.2 and 8.0%, respectively, if the incorporation efficiencies of TMIn and TMGa are kept the same as when the lattice-matched InGaAs is grown on the InP substrate. With the increase in the TMGa supply, the PL wavelength shifts to a shorter wavelength of ~1.35 μm. The addition of Ga into the In(Ga)As QDs induces in two effects. The bandgap energy of the QD material becomes larger so the transition energy between the electron states and the hole states becomes larger and the luminescence wavelength becomes shorter. Conversely, the incorporation of Ga reduces the lattice mismatch between the QD material and InP substrate and the size of the growing QDs gets then lager, resulting in smaller quantized subband energies of the electrons and holes.

The change in the size of the QDs with Ga is seen and measured in the AFM images in Fig. 7. It is shown in Figs. 7(a) - (c) that the sizes of the QDs increase and the areal densities decrease with the addition of Ga. The average lateral size was measured to increase from 50 nm (QD3977) to 56 (QD3979) and 66 nm (QD3972). Moreover, the areal density decreases from 2.4×10^{10} cm^{-2} to 1.2×10^{10} and 2.4×10^{9} cm^{-2}. In contrast, the average height was measured to decrease from 6.6 nm to 6.3 and 4.5 nm. These results indicate that the reduced lattice mismatch between the QD material and InP with the addition of Ga into the InGaAs QDs cause the lateral size of the QD to become larger. However, as the supplied alkyls were consumed while making the lateral size larger, the overall height and the density of the QDs were reduced. An increase in the lateral size would cause the luminescence wavelength to be longer, and a reduction in the height would move the luminescence wavelength to shorter wavelengths. The experimental results shown in Fig. 6 indicate that the effects of increasing the transition energy between the quantized energy states of the electrons and holes through the increase in the bandgap energy of QD semiconductors and the reduction in the height are larger than the effects due to the increase in the lateral size leading to a shift in the luminescence to longer wavelength.

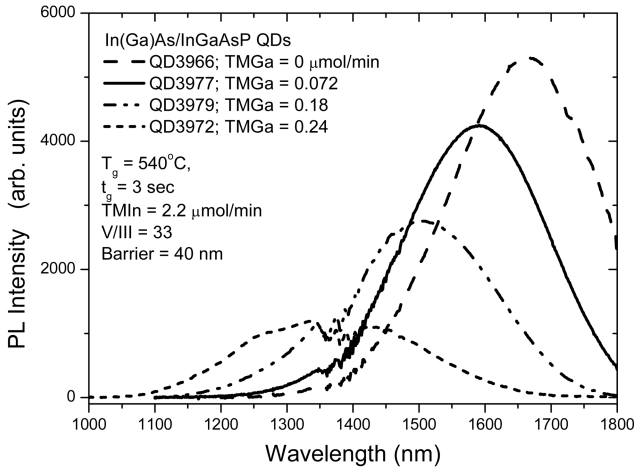

Fig. 6. PL spectra of the In(Ga)As/InGaAsP QDs at room temperature grown with various TMGa supplies.

It is shown that as the concentration of the TMIn increases, the QD density increases. In Fig. 7(d), an AFM image of the five-stack InGaAs/InGaAsP QDs (QD4103) grown at 540 °C for 1 sec with 10 μmol/min of TMIn and 0.072 μmol/min of TMGa is shown. These amounts of TMIn and TMGa result in a Ga mole fraction of 0.6% if the incorporation efficiencies of TMIn and TMGa are held identical to those of the lattice-matched InGaAs grown on InP substrate. The areal density is shown to increase to 8.0×10^{10} cm^{-2}. The average lateral size and height are 35 nm and 4.6 nm, respectively. Therefore, as compared to QD3977, that emits light at approximately 1.59 μm as does QD4103, the QD areal density has increased by a factor of 3.3 and the lateral size and height have each decreased by ~30%. These phenomena can be interpreted as follows: The higher concentration of group III alkyls, mainly TMIn in this case, which is represented by the number of alkyl molecules supplied per unit time by a factor of ~4.5 supplied during the growth of QD4103 as

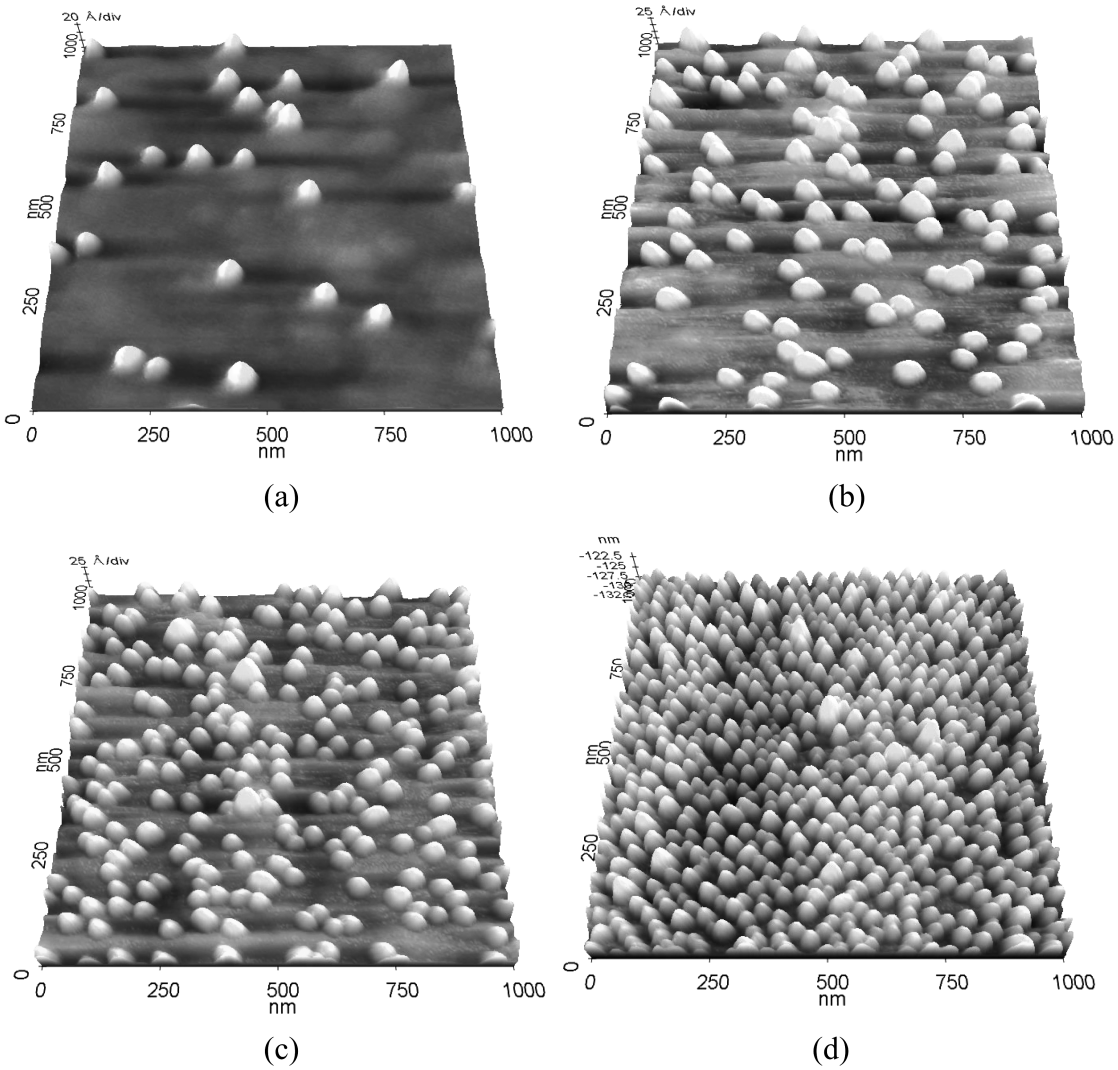

Fig. 7. AFM images of the QDs. (a) QD3977, (b) QD3979, (c) QD3972, the PL spectra of which are shown in Fig. 6. (d) QD4103 grown with a higher concentration of TMIn.

compared to QD3977, causes a larger number of QDs to nucleate. As a result, the QD density increases. As the group III alkyls are being consumed to create a larger number of QDs, the supply of group III alkyls is insufficient to make each QD grow as large as in QD3977. With an increase in the concentration of the TMIn in QD4103, the room-temperature PL peak intensity has increased by a factor of 2.5 as compared to QD3977 with a comparable FWHM.

In Fig. 8(a), the PL spectra of the five-stack InGaAs QDs (QD4547) measured at 10 K and room temperatures are shown. QD4547 was grown in identical conditions to QD4103, except it had a longer growth time of 2.5 sec and had InGaAsP with a smaller bandgap energy (λ_g = 1.1 μm) to control the emission wavelength. The top QD layer is capped with InGaAsP. A FWHM of 32 meV was measured for the 10 K PL spectrum. The narrow PL linewidth without luminescence from the wetting layer at 10 K indicates that the grown QDs are of fairly uniform size and of a high crystal quality, as the PL spectrum at a low temperature is proportional to the density of states in the ground state at a sufficiently low excitation level. In Fig. 8(b), the integrated PL intensity and the FWHM of the spectra are shown as a function of temperature. The PL yield at room temperature is as high as 21% of that at 10 K, indicating that the grown QDs are of high quality. In Fig. 8(c), the room temperature PL spectrum of QD4547 is compared with that of high quality InGaAs/InP QWs that are routinely processed to high performance laser diodes. The PL peak intensity of QD4547 is nearly 30% of that of QW, and the FWHM is 60% larger. This indicates that although the grown QDs are of high crystal quality, as discussed with the results in Fig. 8(a) and (b), the uniformity in size and shape and the quality of the QDs

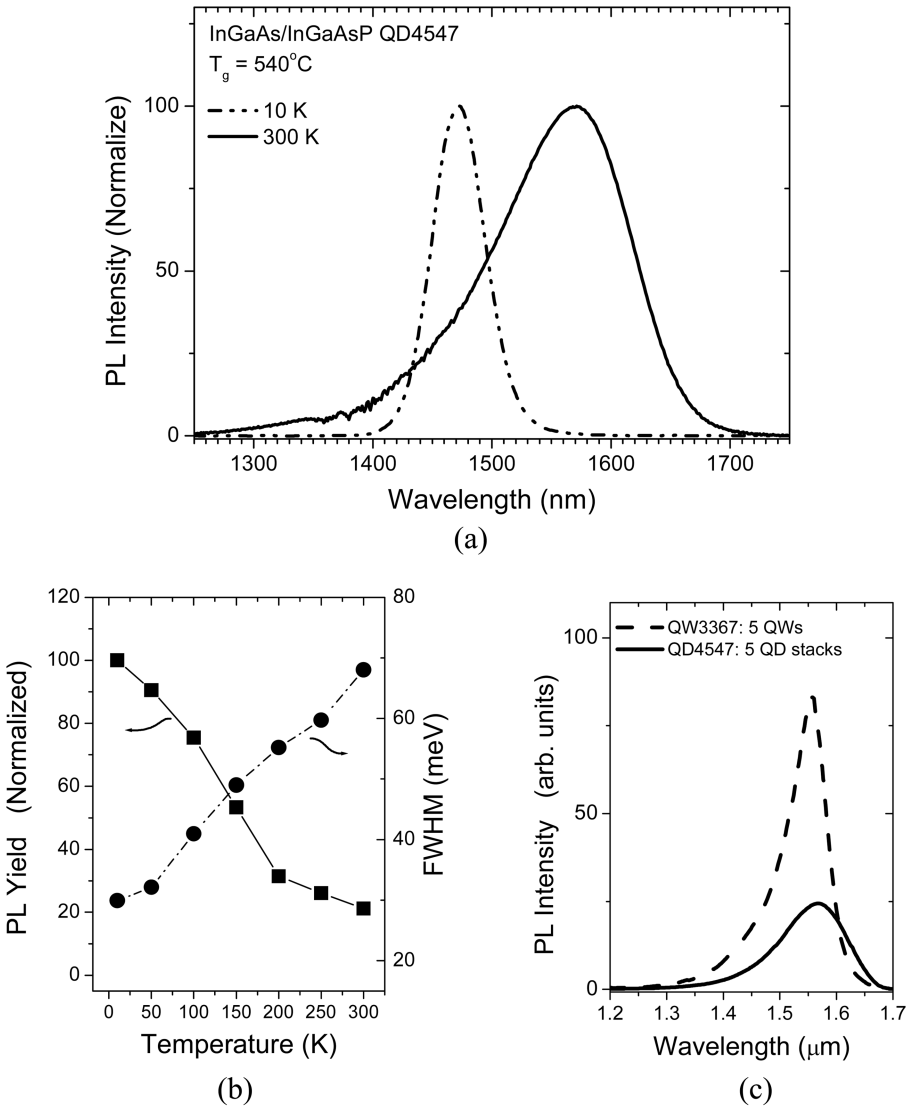

Fig. 8. PL characteristics of QD4547. (a) 10 K and room temperature PL spectra, (b) PL yield and FWHM of the spectrum at different temperatures, (c) PL spectrum of QD4547 as compared to a QW of high optical quality.

should be further optimized in order to show stronger and sharper luminescence.

In Fig. 9(a), the 10 K PL spectra taken from the grown InGaAs/InGaAsP/InP QDs (QD4441) under two excitation powers differing by a factor of 10 are shown. A wavelength of 514 nm from an Ar laser was used, and the reference power in the figures is 10 mW. The QDs were grown at 540 °C for 2.2 sec with 10 μmol/min of TMIn and 0.037 μmol/min of TMGa under a V/III ratio of 5. These amounts of TMIn and TMGa supply result in a Ga mole-fraction of 0.6%. Even with the difference in excitation power by a factor of 10, the changes in the shape and peak position in the PL spectrum is very small. This contrasts to the PL spectra taken from InGaAsP/InP QWs, as shown in Fig. 9(b). The QW PL spectrum moves to shorter wavelengths with the PL excitation power. As QW is physically continuous in the planar direction, the carriers in a QW can move and relax to lower energy states if the carriers can find those states before being recombined. Therefore, the carriers are distributed under a quasi-thermal equilibrium state in each of the conduction and valence bands. More specifically, the luminescence spectrum is homogeneously broadened. As the excitation becomes stronger and additional carriers are generated, the carriers fill up the low energy states and populate the higher energy states as well. This causes a shift of the PL spectrum to the shorter wavelength. However, the carriers in the electrically isolated QDs are confined in their individual host QD. Thus, though there may be lower energy states in other QDs, the carriers cannot move and relax to those states unless the thermal energy is large enough to thermalize the

carriers to escape from the QD and move to the other QDs before being recombined. That is, the luminescence spectrum is inhomogeneously broadened. Therefore, the carriers are distributed in low and excited energy states in various isolated QDs, depending on in which QD the carriers are captured. For the QDs in Fig. 9(a), the spread of the carriers in different energy states results in a PL FWHM of ~35 meV at 10 K. As the excitation power increases, newly generated carriers start to fill up the unoccupied low energy state first, and then fill the higher energy states in each QD. However, unless the number of carriers generated is large enough so that a large number of excited states of individual QD are populated, and the difference in the recombination energy between the excited states and that between the ground states of the conduction and valence bands is in the order of the spectral width of the PL spectrum, the change in the PL spectrum will be small. The spectral change seen in Fig. 9(a) shows typical characteristics of QDs, showing that the light emitting identities in the sample are electrically isolated

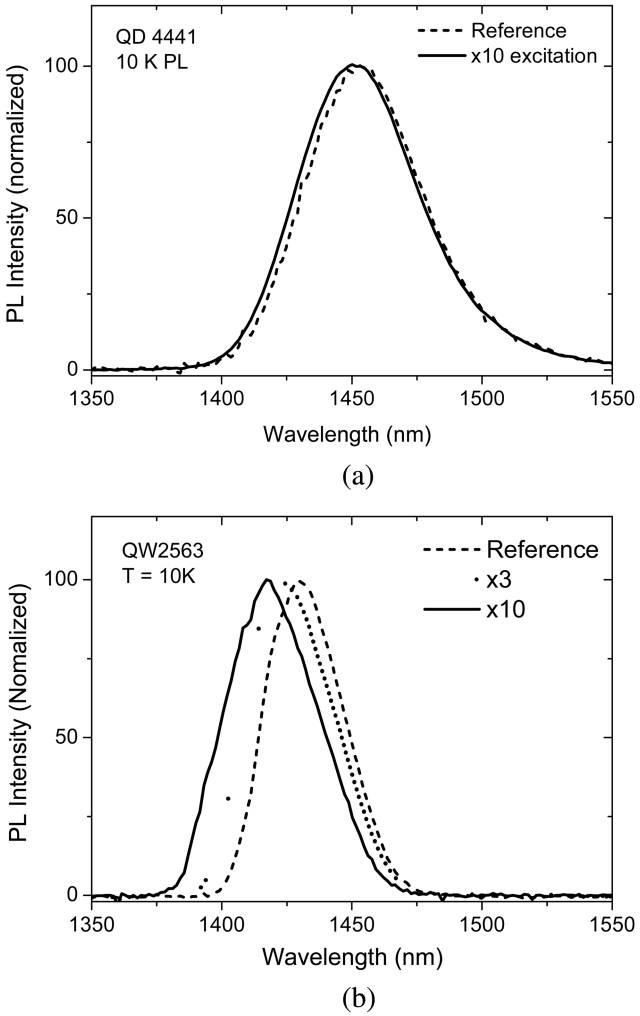

Fig. 9. PL spectra of QD4547 under three different excitation powers.

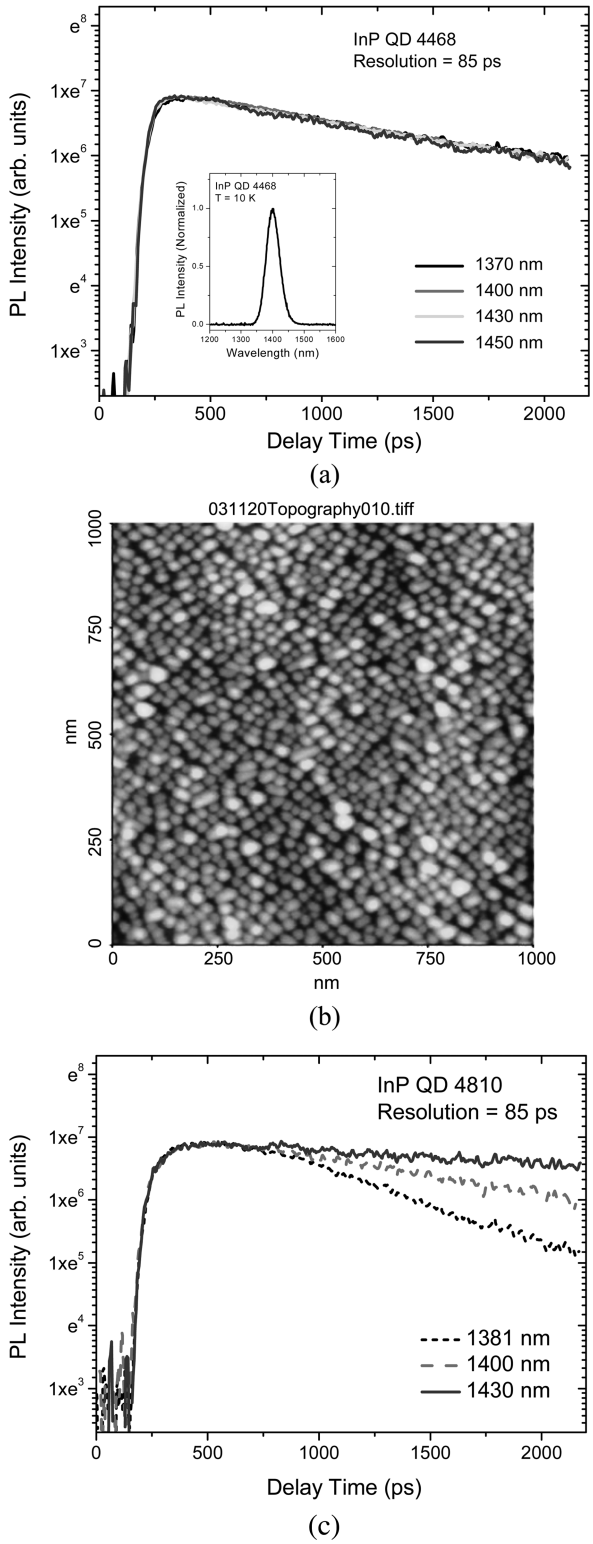

Fig. 10. (a) TRPL decay curves for QD 4468. Across a full PL band of 110 nm, the decay times are identical at ~1.8 ns. (b) An AFM image of QD4468. The QDs were grown with an areal density of 1.1 x 10^{11} cm^{-2}, and an average lateral size and height of 32 nm and 3.4 nm, respectively. (c) TRPL decay curves for QD4810 that has the 15 nm thick InGaAsP spacer layer between the QD stacks. The spacer thickness for QD 4468 is 40 nm.

QDs.

The electrical isolation of the grown QDs is also shown in the time-resolved PL (TRPL), as shown in Fig. 10. The TRPL were carried out with a picosecond streak camera and 2 ps mode-locked pulses from a Ti: sapphire laser. The PL decay curves that represent the decay in the number of carriers were measured with bandpass filters each with a 30 nm band-width. The excitation wavelength was 750 nm, and the average excitation intensity was chosen to be 40 W/cm^2, at which the decay characteristics are identical when the intensity is further decreased. In this way, it was possible to avoid the contribution of carriers from the higher energy states due to the high carrier density, while at the same time it was possible to obtain the best signal-to-noise ratio. The carrier lifetimes were measured to be ~1.8 ns across the entire PL band of 110 nm for QD4468. This observation attests to the negligible lateral electronic coupling between the dots. If the QDs are electrically coupled, the carriers will move to the lowest energy states that they can find in the neighboring QDs. Therefore, the number of carriers occupying the high energy states will decrease faster than that in the lower energy states. However, the similar decay time across the PL band of 110 nm indicates that this type of carrier transfer does not occur. In fact, the QD has a very high areal density. As shown in Fig. 10(b) the QD shows an areal density of 1.1×10^{11} cm^{-2} with an average lateral size and height of 32 nm and 3.4 nm, respectively. This areal density is one of the highest densities ever achieved for III-V compound semiconductors. The TRPL data in Fig. 10 show that even as the lateral dot separation (~ 30 nm) becomes comparable to the dot size (~30 nm), the lateral electrical coupling is negligible and the QDs are electrically well isolated.

However, when the QDs are grown closely in a vertical direction, coupling occurs. In Fig. 10(c), the TRPL of QD4810 is shown. QD4810 was grown to have five QD stacks separated by a 15 nm-thick InGaAsP spacer layer. The separation between the QD stacks in QD4468 is 40 nm. In Fig. 10(c), it is shown that the number of carriers with high energy decays much faster than that with low energy. This shows that the carriers with high energy have transferred to a low energy state in the neighboring QDs. These results for TRPL indicate that the coupling between the QDs, and thus, the degree of inhomogeneous broadening can be controlled by the thickness of the spacer layer in a QD multistack.

6. EXPERIMENTAL RESULTS ON QD LDS AND QD SOAS

The grown QDs were used as the active media of QD LDs and as a semiconductor optical amplifier (SOA) and the device performances were analyzed. For the LD and SOA structures, a 200 nm-thick InP buffer and a 1.1 μm-thick InP

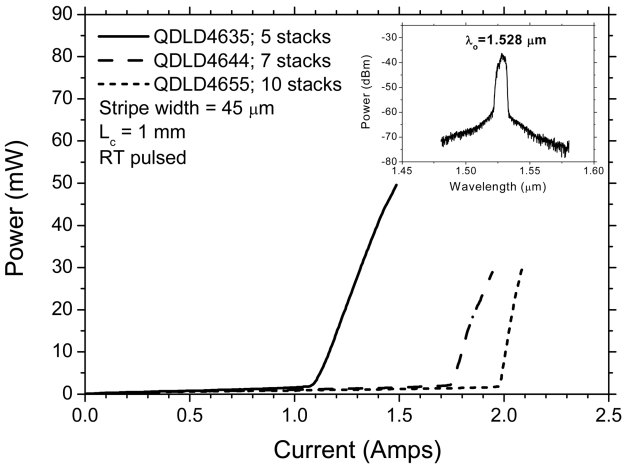

Fig. 11. L-I characteristics of InGaAs/InGaAsP/InP QD broad area lasers with 5, 7, and 10 QD stacks at room temperature. In the inset, the lasing spectrum of a 10 QD stack laser is shown.

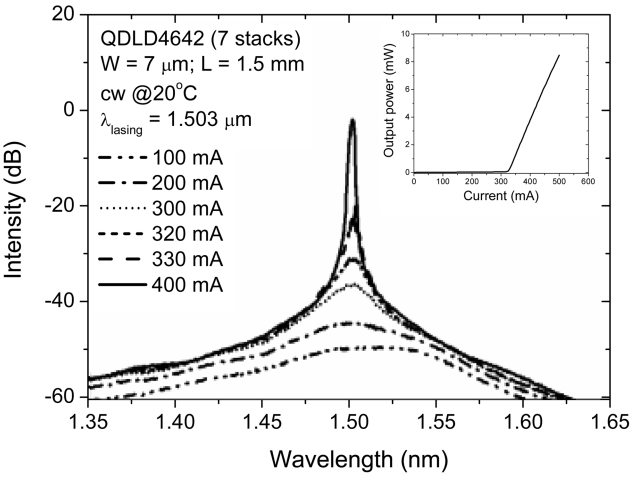

Fig. 12. Lasing spectrum of InGaAs/InGaAsP/InP QD LD with 7 QD stacks under a cw mode at 20 °C.

clad were grown on an n-InP substrate at 620 °C. The temperature was then lowered to the QD growth temperature, and the InGaAsP (λ_g = 1.1 μm) waveguide layers and QDs were grown. The thickness of the waveguides on both sides of the QD multistacks were 100 nm, and the QD stacks were separated by 40 nm thick InGaAsP (λg = 1.1 μm) barriers. Following the QD multistacks and the upper InGaAsP waveguide layer, a 1.3 μm-thick InP clad and a 100 nm-thick InGaAs contact layer were grown. This structure is drawn schematically in Fig. 4(b).

The room temperature light-current (LI) characteristics of InGaAs/InGaAsP/InP QD broad area lasers under a pulsed operation are shown in Fig. 11. The InGaAs QDs in the lasers were grown with 8 μmol/min of TMIn and 0.072 μmol/min of TMGa for 2.7 sec. The stripe width and the cavity length are 45 μm and 1 mm, respectively. The pulse width was

1 μsec, and the pulse was repeated every 150 μsec. The QD LDs with 5, 7 and 10 QD stacks lase at wavelengths between 1.484 - 1.528 μm, with longer wavelengths corresponding to a larger number of QD stacks. This is believed to be caused by the difference in the energy states generating gain. It will be discussed in more detail later in this paper. The minimum threshold current densities of QD4635 with five QD stacks and QD4644 with seven QD stacks were measured at 2.2 and 3.0 kA/cm^2, respectively, for cavity lengths in a range of 300 - 1000 μm. These correspond to threshold current densities per QD stack of 440 and 430 A/cm^2, respectively. From the LI and threshold current density measurements at cavity lengths between 300 - 1000 μm, it was determined that the transparency current density is ~100 A/cm^2 per QD stack for QD4635 and QD4644. The slope efficiencies at a 1 mm cavity length were measured to be 0.16 and 0.13 mW/mA for the five- and seven-stack lasers, respectively.

These measured threshold current densities for the QD LDs are higher and the slope efficiencies are lower than those of typical QW lasers and In(Ga)As/GaAs QD lasers. This indicates that the growth conditions for the QDs should be further optimized. However, these results demonstrate that a room-temperature lasing operation at 1.5 μm has been realized from round, dome-shaped InGaAs QDs on (100) InP substrates with lattice-matched InGaAsP barriers. These results are contrast with previous reports in which the active media responsible for the optical gain assumes a quantum-dash form, that lasing was possible only with QDs grown on (311) substrates, or that tensile-strained GaAs underlayers should be used to obtain a high QD luminescence efficiency[28-30].

The lasing spectrum from a ridgewaveguide (RW) QD LD (QDLD4642) with seven QD stacks in the active region and a ridge width of 7 μm and a cavity length of 1.5 mm is shown in Fig. 12. The InGaAs QDs were grown with 8 μmol/min of TMIn and 0.037 μmol/min of TMGa for 2.7 sec under a V/III ratio of 5. These amounts of TMIn and TMGa result in a Ga composition of 0.7%. It is shown that the lasing occurs at 1.503 μm under a cw mode with a threshold current of ~325 mA at 20°C. In addition to the main peak, shoulders are seen at ~1.535 μm at 100 and 200 mA in the electroluminescence (EL) spectra. The intensity of the main peak at ~1.505 μm becomes stronger as the injection current increases. The shoulder peaks are believed to have originated from the optical transition between the ground states of the electrons and holes in the QDs. The lasing occurs mostly through the transitions between excited states of electrons and holes in the QDs where the gain is larger due to a larger density of states, as can be explained below.

The energy shift of the lasing peak from the EL shoulder at 100 mA in Fig. 12 is approximately 17 meV, while the spectral width of the room temperature PL spectrum of the QDs grown under similar conditions is nearly 60 meV as in Fig. 8(a). This spectral width is more than two times larger than that typically measured from high quality 1.55 μm InGaAsP/InP quantum wells. The broader spectral width results from the spread in the size and shape of the grown QDs. Although the joint density of states of an individual QD is of a delta-function nature, the quantized energies of electrons and holes in each QD are different, and the difference in transition energies causes the PL spectrum 60 meV to be wide. That is, the luminescence spectrum is inhomogeneously broadened. As the EL peak at 100 mA is located at 1.535 μm, the corresponding energy is close to the transition energy between the ground states of electrons and holes in the QDs with the same size and shape. These constitute the largest number in the QD ensemble with different sizes and shapes. The fact that the lasing then occurs at an energy higher by 17 meV compared to the transition energy between the electron and hole ground states that have densities of states of delta-function natures of the largest group of QDs indicates that the energy states involved in producing the gain for the lasing are mostly from the excited states with a small contribution from ground states at the lasing energy.

A similar shift in the lasing wavelength is observed from QD LDs with different number of QD stacks and cavity lengths. The lasing spectra of a QD LD (QDLD4645) with 10 QD stacks under a pulsed mode are shown in Fig. 13. When the cavity length is 390 μm, the lasing occurs at 1.478 μm. When the cavity length is 1 mm long, the lasing wavelength becomes 1.508 μm. The modal mirror loss in a 390-μm-long QD LD is ~18 cm^{-1} larger than that in a 1-mm-long QD LD, and a larger gain is needed in order to reach the threshold. It is believed that the carriers have been pumped to higher excited states in order to obtain a larger gain; thus, the lasing wavelength is shifted to a shorter wavelength. In

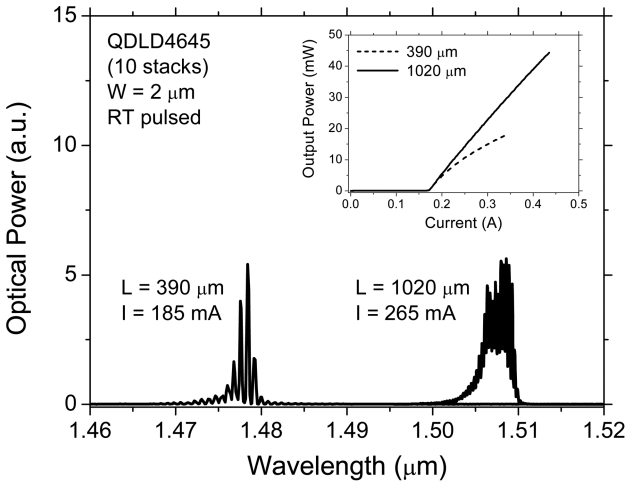

Fig. 13. Lasing spectra of InGaAs/InGaAsP QD LD with 10 QD stacks under a pulsed mode. The lasing wavelength shifts to shorter wavelength when the cavity length is short.

the inset of Fig. 13, it is shown that the threshold currents of two QD LDs are nearly identical, although the cavity lengths are different by a factor of 2.5. This once again suggests that the energy states involved in producing the gain are different in the two QD LDs. A larger number of carriers are being pumped to higher excited states for the 390 mm long QD LDs.

The cw lasing spectrum at room temperature for the QD LDs (QDLD4635) with five QD stacks and a cavity length of 400 μm is shown in Fig. 14. It is shown that the lasing occurs at 1.445 μm, suggesting that the lasing occurs through excited states of inhomogeneously broadened QD energy states. When the number of QD stacks is increased to 15, the lasing wavelength shifts to 1.56 μm, as shown in Fig. 15. As the gain obtainable from the ground states of the QDs increases and the carrier capture in the QDs becomes more efficient with an increase in the number of QD stacks, larger gain is obtained from the ground states of the QDs with the increase in the number of QD stacks. The number of excited states needed to obtain enough gain for lasing would then decrease. This is believed to be the reason that the lasing wavelength moves to a longer wavelength for the QD LDs with 15 QD stacks. The same logic can be applied to explain the shift in the lasing wavelength in Fig. 11.

Although the QD LD performances are not as good as those obtainable from QW LDs due to the wider luminescence spectrum caused by nonuniformity among the QD sizes and compositions, the broad inhomogeneously broadened spectrum is beneficial for a SOA operation. When bulk

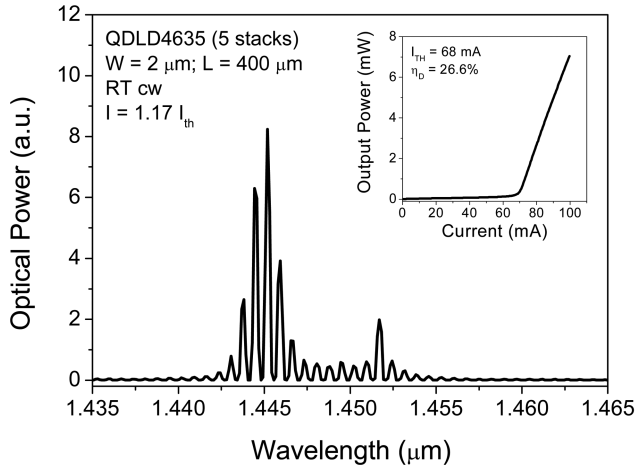

Fig. 14. Lasing spectra of InGaAs/InGaAsP/InP QD LD with 5 QD stacks under a cw mode at room temperature. The lasing occurs at a very short wavelength of ~1.445 μm.

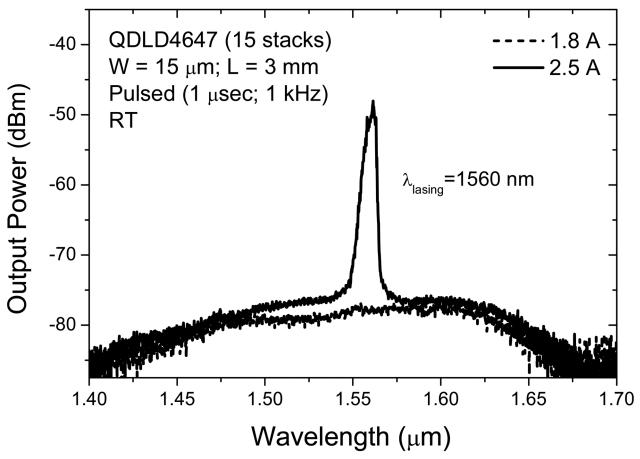

Fig. 15. Lasing spectra of a QD LD with 15 QD stacks. The lasing wavelength has moved to long wavelength of 1.56 μm. It is believed that the long wavelength lasing occurs mostly through a transition between the ground states of the electrons and holes in inhomogeneously broadened QDs.

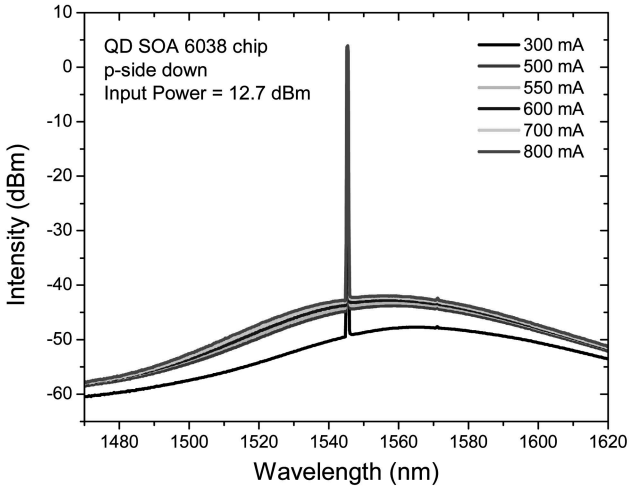

(a)

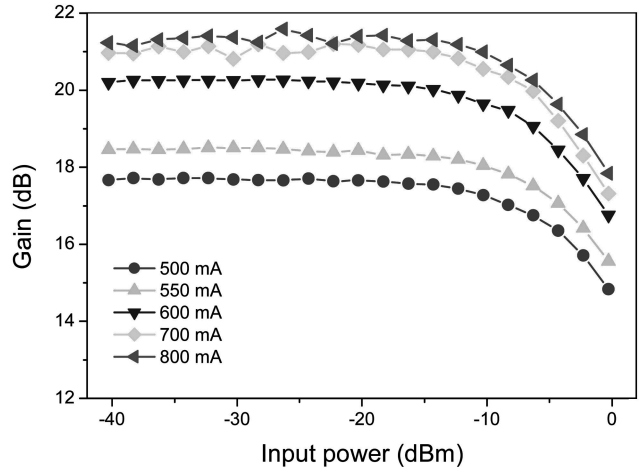

(b)

Fig. 16. (a) Optical amplification spectra of the fabricated RW QD SOA. (b) Measured gain as a function of optical input power. A small signal gain of 17.7 dB is measured at an injection current of 500 mA.

semiconductors or QWs are used as the gain medium for the SOA, an amplification of the optical signal at one wavelength causes a change in the gain at the other wavelength. That is, crosstalk occurs. This is caused by carrier movement toward the lower energy states in the bulk semiconductors and QW layers. Once the carriers are consumed by the amplification of one input optical signal, the carriers that have different energies attempt to move to the energy states of the consumed carriers. The gain at the moving carriers' original energy states is thus reduced. This crosstalk has been the central problem hindering a wider use of SOA for optical fiber communication systems. However, with the QDs well isolated electrically from each other, the carrier movement will not occur, thus the gain will not be changed although the carriers were consumed when the input signal was amplified. Only hole burning in the gain spectrum occurs at the input signal wavelength. In addition, it has been reported that the gain recovery with QDs is much faster than with QWs. Furthermore, the gain saturation power is much larger. In order to exploit this beneficial property of QDs, QD SOAs were fabricated.

In Fig. 16(a), the amplification spectrum is shown of the fabricated RW QD SOA 6038 with five QD stacks and a cavity length of 2.5 mm. The RW QD SOA is mounted p-side down in order to effectively extract the heat generated while driving the SOA. The power of the input signal at 1545 nm was 12.7 dBm. In the figure, it is clear that the input signal has been amplified while passing through the SOA and that the output signal becomes stronger with a higher current injection into the SOA. From the SOA spectrum, the SOA gain as function of the input power is calculated and plotted in Fig.16(b). The small signal gain of the fabricated QD SOA is measured to be nearly 17.7 dB with an injected current of 500 mA.

7. CONCLUSION

In summary, the MOCVD growth condition was optimized and InGaAs/InGaAsP QDs emitting at around 1.55 μm were grown. The grown InGaAs/InGaAsP QDs have a round, domed shape, and areal densities as high as 1.1×10^{11} cm^{-2} were obtained. The grown QDs show high optical quality with a narrow FWHM and a high PL intensity attesting to this. A power-dependent PL and a time-resolved PL show that the grown QDs are electrically isolated from each other, thus the PL spectrum is inhomogeneously broadened.

Using the grown QDs as active media for QD LDs and QD SOA, a high device performance was demonstrated. The QD LDs with five and seven QD stacks have lased cw at room temperature. It was shown that as the cavity length becomes longer and the number of QD stacks becomes larger, the lasing wavelength shifts to a longer wavelength. It is analyzed that this is due to a decreasing mirror loss with a longer cavity and an increasing gain with a larger number of QD stacks, so that the lasing occurs either through a ground state or an excited state depending on the modal gain required. In addition, with 15 QD stacks, the lasing was achieved at 1.56 μm. All of these figures are among the best results ever obtained for InP-based QDs.

However, the measured optical qualities of the FWHM in addition to the PL intensity of QDs do not yet measure up to those of the QWs. This is principally due to nonuniformity among the QD sizes and compositions. This nonuniformity spreads out the luminescence spectrum of the QDs. It is required that the growth condition should be further optimized in order to control the size and composition of QDs in a much narrower range so that the advantages of ideal QDs may be exploited to enhance the performance of QD devices.

Nonetheless, a nonuniformity in QD size and composition as well as the resulting broad inhomogeneous broadened luminescence spectrum is beneficial for SOA operations. The inhomogeneous broadening will reduce the cross-talk for SOA. QD SOAs were fabricated, and a small signal gain of 17.7 dB and a gain bandwidth of 45 nm were achieved. This indicates that the QD growth condition has been optimized for the growing of high-quality QD SOAs.

ACKNOWLEDGEMENTS

The works presented in this paper are the results of collaborations with other researchers. The author appreciates the work done by graduate students S. H. Pyun and J. W. Jang at the Semiconductor Epitaxy and Device Laboratory at Sungkyunkwan University. In addition, the author is grateful for the collaboration with Professor D. Lee and his graduate students in the Department of Physics at Chungnam National University.

This work was supported by the National Research Laboratory program (Grant No. 2004-02403) in Korea.

REFERENCES

1. H. M. Manasevit, *Appl. Phys. Lett.* **12**, 156 (1968).
2. R. D. Dupuis and P. D. Dapkus, *Appl. Phys. Lett.* **31**, 466 (1977).
3. R. D. Dupuis and P. D. Dapkus, *Appl. Phys. Lett.* **31**, 406 (1978).
4. N. J. Nelson, K. K. Johnson, R. L. Moon, H. A. Vander Plas, and L. W. James, *Appl. Phys. Lett.* **32**, 26 (1978).
5. N. Holonyak Jr., R. M. Kolbas, R. D. Dupuis, and P. D. Dapkus, *Appl. Phys. Lett.* **33**, 73 (1978).
6. R. D. Dupuis, P. D. Dapkus, C. M. Garmer, C. Y. Su, and W. E. Spicer, *Appl. Phys. Lett.* **34**, 335 (1979).
7. M. J. Ludowise, *J. Appl. Phys.* **58**, R31 (1985).

8. R. D. Dupuis, *IEEE J. Select. Top. Quantum Electron.* **6**, 1040 (2000).
9. J. J. Coleman and P. D. Dapkus, *Gallium Arsenide Technology* (eds. D. K. Ferry), p.79-105, SAMS (1985).
10. Z. I. Alferov, V. M. Andreev, V. I. Korol'kov, E. I. Portnoi, and A. A. Yakovenko, *Fiz. Tekh. Poluprovodn,* **3**, 930 (1968).
11. I. Hayashi, M. B. Panish, P. W. Foy, and S. Sumski, *Appl. Phys. Lett.* **17**, 109 (1970).
12. Z. Alferov, *IEEE Select. Top. Quantum Electron.* **6**, 832 (2000).
13. L. A. Coldren and S. W. Corzine, *Diode Lasers and Photonic Integrated Circuits,* p.488-507 (1995).
14. L. A. Coldren and S. W. Corzine, *Diode Lasers and Photonic Integrated Circuits,* p.527-536 (1995).
15. F. Schwierz and J. J. Liou, *Modern Microwave Transistors,* p.121-162 (2003).
16. D. L. Huffaker and D. G. Deppe, *Appl. Phys. Lett.* **73**, 520 (1998).
17. K. Nishi, H. Saito, S. Sugou, and J. Lee, *Appl. Phys. Lett.* **74**, 1111 (1999).
18. K. Mukai, Y. Nakata, K. Otsubo, M. Sugawara, N. Yokoyama, and H. Ishikawa, *IEEE J. Quantum Electron.* **36**, 472 (2000).
19. Y. Arakawa and H. Sakaki, *Appl. Phys. Lett.* **40**, 939 (1982).
20. W. G. Jeong, P. D. Dapkus, U. H. Lee, J. S. Lim, D. Lee, and B. T. Lee, *Appl. Phys. Lett.* **78**, 1171 (2001).
21. U. H. Lee, J. S. Lim, D. Lee, W. G. Jeong, E. H. Hwang, D. Y. Lee, J. S. Shim, P. D. Dapkus, and R. Stevenson, *Jpn. J. Appl. Phys.* **41**, 524 (200).
22. J. W. Jang, S. H. Pyun, S. H. Lee, I. C. Lee, W. G. Jeong, R. Stevenson, P. D. Dapkus, N. J. Kim, M. S. Hwang, and D. Lee, *Appl. Phys. Lett.* **85**, 3675, (2004).
23. S. H. Pyun, S. H. Lee, I. C. Lee, H. D. Kim, W. G. Jeong, J. W. Jang, N. J. Kim, M. S. Hwang, D. Lee, J. H. Lee, and D. K. Oh, *J. Appl. Phys.* **96**, 5766, (2004).
24. H. D. Kim, W. G. Jeong, J. H. Lee, J. S. Lim, D. Lee, R. Stevenson, J. W. Jang, and S. H. Phyu, *Appl. Phys. Lett.* **87**, 083110 (2005).
25. H. D. Kim and W. G. Jeong, *J. Korean Phys. Soc.* **47**, 5 (2005).
26. Y. D. Jang, E. K. Lee, D. Lee, W. G. Jeong, S. H. Pyun, and J. W. Jang, *Appl. Phys. Lett.* **88**, 091920 (2006).
27. N. J. Kim, Y. D. Jang, J. S. Lim, J. H. Lee, D. Lee, S. H. Pyun, W. G. Jeong, and J. W. Jang, K. *Korean Phys. Soc.* **48**, 1210 (2006).
28. R. H. Wang, A. Stintz, P. M. Varangis, T. C. Newell, H. Li, K. J. Malloy, and L. F. Lester, *IEEE Photon. Technol. Lett.* **13**, 767 (2001).
29. R. Schwertberger, D. Gold, J. P. Reithmaier, and A. Forchel, *IEEE Photon. Technol. Lett.* **14**, 735 (2002).
30. H. Saito, K. Nishi, and S. Sugou, *Appl. Phys. Lett.* **78**, 267 (2001).